Evolution and structural transition of quasicrystalline phases in Al-Fe-Cu-Cr and Al-Fe-Cu-Mn alloys during high energy ball milling

Journal of Physics: Conference Series **226** (2010) 012009 doi:10.1088/1742-6596/226/1/012009

Evolution and structural transition of quasicrystalline phases in Al-Fe-Cu-Cr and Al-Fe-Cu-Mn alloys during high energy ball milling

Thakur Prasad Yadav[1], Nilay Krishna. Mukhopadhyay[2*], Radhey Shyam Tiwari[1], and Onkar Nath Srivastava[1]

[1]Department of Physics, Banaras Hindu University, Varanasi-221 005 (INDIA)
[2]Department of Metallurgical Engineering, Institute of Technology, Banaras Hindu University, Varanasi-221 005, (INDIA)

*E-mail:mukho_nk@rediffmail.com

Abstract. The main objective of the current work was to investigate the transformation mechanism in quasicrystals during mechanical alloying/milling. The quasicrystalline phases have been synthesized by melting the individual elements as well as by mechanical alloying of the concerned elements using high energy ball milling. The transformation of icosahedral and decagonal quasicrystalline phases to various disordered states in Al-Fe-Cu-Cr and Al-Fe-Cu-Mn alloys during milling of the pre-alloyed material. The milling of a quasicrystalline alloy was carried out using a high energy ball mill by varying milling times up to 40h under liquid hexane medium and at various milling intensity. X-ray diffraction was carried out for evaluating the lattice strain, lattice parameters and crystallite sizes of the mechanically milled samples. The evolution of nano icosahedral and nano decagonal phases as well as crystalline phases was found to occur. The subsequent thermal treatment led to the structural ordering in the concerned phases. The implication of the evolution of various phases, their structural correlations and their relative stability will be discussed.

1. Introduction

Quasicrystals (QC) have well-ordered structures without periodicity, and exhibit noncrystallographic rotational symmetries (e.g. five-fold, eight-fold, ten-fold and twelve- fold) as well as crystallographic rotational symmetries [1-4].

Due to the aperiodicity, these materials are expected to exhibit properties that are very different from conventional metallic materials and these properties can be exploited for industrial applications [5-10]. The stability of quasicrystalline materials during mechanical milling (MM) appears to be important as they can give rise to other stable/metastable phases [11]. The icosahedral phase in A1-Cu-Fe system is of particular interest because it appears to have a very perfect quasicrystalline structure [12]. It is known that QC phase in Al-Cu-Fe undergoes a structural transformation to various types of crystalline phases during MM [13]. The structure of A1-Cu-Fe alloy is sensitive to the additions of other elements such as chromium, manganese which destabilizes the icosahedral phase and promotes the formation of the decagonal and one dimensional quasicrystal [14-15]. It is interesting to emphasize that the stability

of deacagonal and one dimensional quasicrystal should be examined during MM. As it is possible to obtain a nanoscale microstructure after MM, which may lead to the formation of equilibrium or stable phases in the Al-Cu-Fe-Cr and Al-Cu-Fe-Mn systems.

The aim of the present investigation is to synthesize a decagonal phase in $Al_{65}Cu_{20}Fe_7Cr_8$ and one dimensional quasicrystal in $Al_{65}Cu_{20}Fe_7Mn_8$ alloy system and to study its phase stability during mechanical milling. An isothermal heat treatment in vacuum and air was also investigated in order to study the possible formation of spinel structure.

2. Experimental Procedure

Alloys with a composition close to $Al_{65}Cu_{20}Fe_7Cr_8$ and $Al_{65}Cu_{20}Fe_7Mn_8$ (Al=99.98%, Cu=99.99%, Fe = 99.98 % Cr=99.97%, Mn = 99.92 % pure) were prepared by melting in an R.F. induction furnace under a dry argon atmosphere. The individual elements were at first mixed in correct stoichiometric proportions and pressed into a cylindrical pellet of 2 cm diameter and 0.75 cm thickness by applying a pressure of $\sim 3 \times 10^4$ N/m^2. The pellet (5 g by weight) was then placed in a silica tube surrounded by an outer pyrex glass jacket. Under continuous flow of argon gas into the silica tube, the pellet was melted using radio frequency induction furnace (18 kW). The ingots formed were re-melted several times to ensure homogeneity. This pre-alloyed as cast ingot was crushed to particles less than 0.5mm in size and placed in an attritor ball mill (Szegvari Attritor) with ball to powder ratio of 40:1. The attritor has a cylindrical stainless steel tank of inner diameter 13 cm. The grinding balls made of stainless steel are of 6 mm in diameter. The speed of the mill was maintained at 400 rpm. The milling operation was conducted for various time ranging from 5h to 40h using hexane as a process control agent (PCA). Powders obtained after 40 h of milling was further annealed at 400, 500, 600 700, 800 and 900 ˚C for time ranging from 10 to 60h in air ambient. The air annealing has been done for oxidation of milled powders to form spinel phase. Structural and microstructural characterizations of the mechanically activated and annealed powders were performed using scanning electron microscope (SEM – QUANTA 200), X-ray diffraction (XRD) with CuK_α radiation (Philips PW-1710 X-ray diffractometer, λ =1.54026 Å), scanning electron microscopy (Philips XL-20) and transmission electron microscopy (TEM- Techni G^{20} at 200kV).The effective crystallite size and relative strain of mechanically milled powders as well as heat-treated products were calculated based on line broadening of XRD peaks. The use of the Voigt function for the analysis of the integral breadths of broadened X-ray diffraction line profiles forms the basis of a single line method of crystallite-size and strain determination [17].

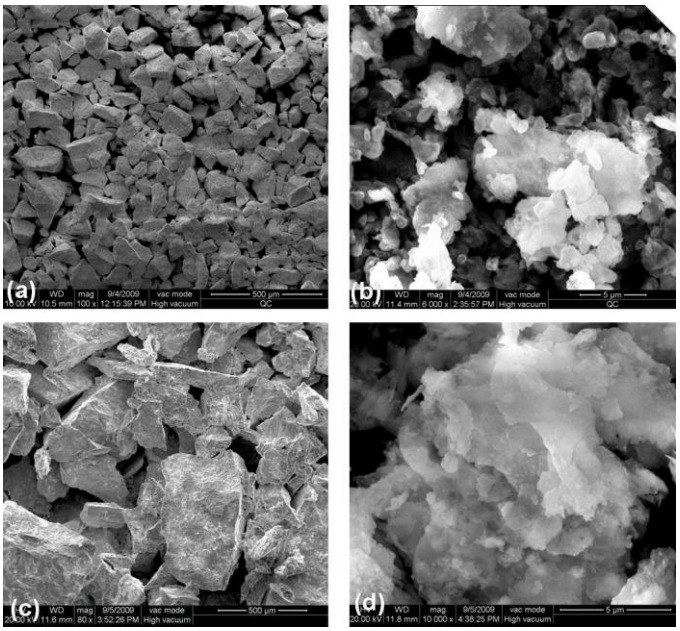

Figure1. Scanning electron microscope images of $Al_{65}Cu_{20}Fe_7Cr_8$ alloy (a) as cast, (b) 40 h milled; $Al_{65}Cu_{20}Fe_7Mn_8$ alloy (c) as cast & (d) 40 h milled.

3. Results and discussions

Fig.1 represents SEM images showing the morphology of (a) as cast, (b) 40 h milled $Al_{65}Cu_{20}Fe_7Cr_8$ alloy; (c) as cast & (d) 40 h milled $Al_{65}Cu_{20}Fe_7Mn_8$ alloy. In both the as cast alloys the μm size particle was observed and after milling, the powders are markedly agglomerated and the coarse particles are formed on the surface of materials, the size of powders tends to be reduced with increasing the MM treatment time. This is due to the formation of nano quasicrystalline / crystalline grain during MM.

In order to investigate the effect of the Cr substitution in place of Fe in Al-Cu-Fe icosahedral phase, the quaternary alloy $Al_{65}Cu_{20}Fe_7Cr_8$ shows the formation of decagonal phase. Fig. 2(a) shows XRD pattern of the decagonal phase obtained from the as cast $Al_{70}Cu_{20}$ Fe_7Cr_8 alloy. The diffraction pattern corresponding to decagonal phase can be indexed by using six independent indices as proposed by Mukhopadhyay and Lord [18]. All of the peaks are from the decagonal phase, no other phase was identified. Fig. 2(b-e) shows the XRD pattern from different hours (10, 20, 40 and 60 h) MM powder exhibiting broadening of the peaks belonging to the B2 phase after 20 h milling. At the initial stage of milling the formation of icosahedral phase coexisting with decagonal phase have been observed (Fig.2 (b)). It should be noted that the shift of the peaks towards lower θ angle side with increase in milling time indicate the increase in lattice parameter of the B2 phase. Intensity of (110) peak goes on decreasing with increasing milling time and it becomes broadened for milling time of 60 hrs ,which clearly evidences formation of amorphous along with B2 phase (see Fig 2(e)). XRD pattern indicate that the initially sharp diffraction lines are considerably broadened after subsequent ball milling, suggesting that the nano- crystalline phase is present in the milled sample and have evolved during milling. The calculated crystallite size (d) as a function of milling time shows a rapid decrease of the crystallite size to 14 nm with milling time up to 60h.

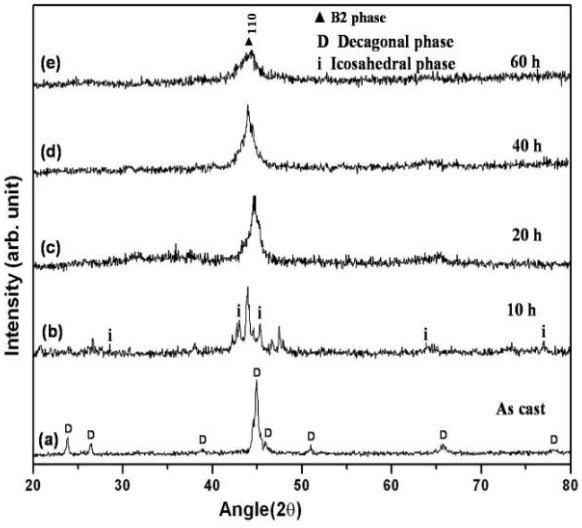

Figure 2. XRD pattern from as cast $Al_{65}Cu_{20}Fe_7Cr_8$ alloy (a) and different hours mechanical milled (10, 20, 40 and 60 h) powder (b-e).

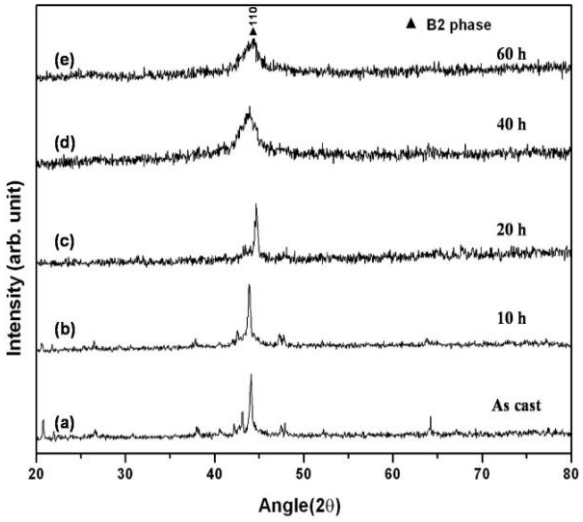

Figure 3. XRD pattern of as cast $Al_{65}Cu_{20}Fe_7Mn_8$ alloy (a) and different hours mechanical milled (10, 20, 40 and 60 h) powder (b-e).

Fig. 3(a) shows XRD pattern of the one dimensional quasicrystal (1DQC) obtained from the as cast $Al_{65}Cu_{20}Fe_7Mn_8$ alloy. Fig. 1(b-e) shows the XRD pattern from mechanical milled (10, 20, 40 and 60 h) powder, exhibiting broadening of the peaks belonging to the B2 phase. From the XRD pattern it is evident that the initially sharp diffraction peaks are considerably broadened after ball milling due to a decrease in the particle size and an increase in internal lattice strains.

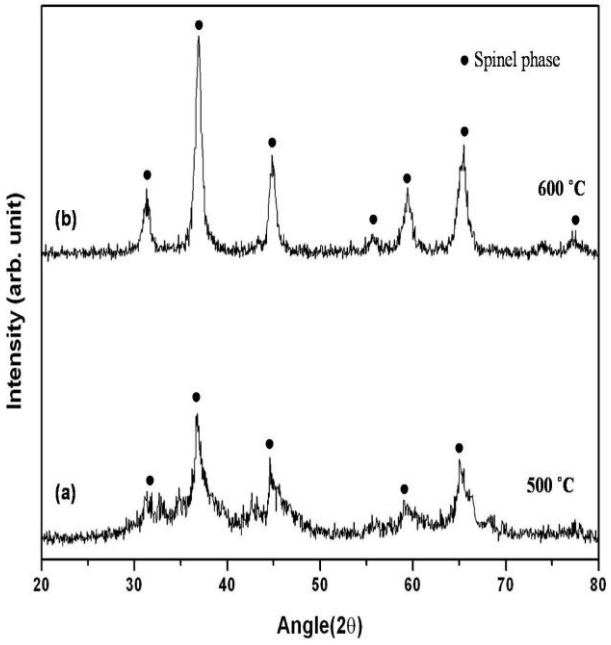

Figure 4. XRD patterns of 40 MM $Al_{65}Cu_{20}Fe_7Cr_8$ powders, air annealing for 60 h at 500 ˚C (a) and 600 ˚C (b).

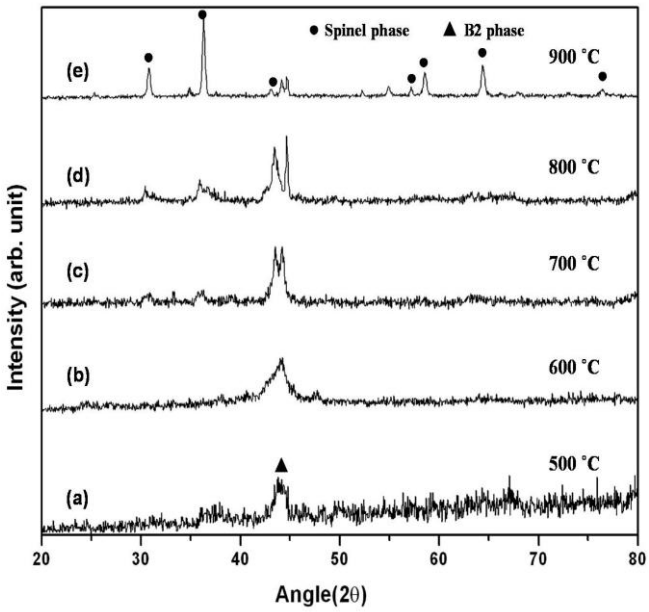

Figure 5. XRD patterns of 40 MM $Al_{65}Cu_{20}Fe_7Mn_8$ powders, air annealing for 60 h at different temperature (a-e).

The investigation on the stability of MM $Al_{65}Cu_{20}Fe_7Cr_8$ alloy has been carried out by annealing in air. In the case of $Al_{65}Cu_{20}Fe_7Cr_8$ MM powder, the formation of single phase spinel has been observed after 60 h of air annealing at 600 ˚C by 40 h mechanically activated powder. XRD patterns (Fig 4(a-b)) show the peaks corresponding to the spinel structure with the lattice parameter 8.05 ±0.04 Å. It is obvious that the high degree of oxidation has caused the formation of $(Fe,Cr)Al_2O_4$ spinel structures from the MM materials. It is understood that after 40h of milling, the surface and interface areas are increased due to the formation of smaller particles as well as the nanocrystallite. The thermal stability of 40 MM $Al_{65}Cu_{20}Fe_7Mn_8$ powder has been also done at same annealing parameter. The rate of formation of spinel phase in $Al_{65}Cu_{20}Fe_7Mn_8$ powders is very slow and B2 phase is still present along with spinel phase up to 900˚ C annealing temperature. When the annealing has been done in air, at different temperatures i.e. 500, 600, 700, 800 and 900 ˚C a significant phase transformation has been found to occur in case of 40 h mechanically activated 1DQC powder. XRD pattern (Fig 5(a-e)) shows the peaks corresponding to the spinel structure with the lattice parameter 8.07 ± 0.04 Å and parent B2 pase with a= 2.9 ± 0.06 Å. It is very interesting ti note that the kinetics of oxidation rate, which is controlled by oxygen diffusion, are not same in both alloy $Al_{65}Cu_{20}Fe_7Cr_8$, $Al_{65}Cu_{20}Fe_7Mn_8$. It should be noted that the oxidation of $Al_{65}Cu_{20}Fe_7Mn_8$ alloy was not insignificant in comparison to that of $Al_{65}Cu_{20}Fe_7Cr_8$ powder after same annealing parameter. This could be due to the higher affinity of Cr for oxygen compared to that of Mn.

The rigorous transmission electron microscopic (TEM) investigation by obtaining selected area diffraction patterns and microstructural features at different stages have been carried out. Fig. 6 shows TEM investigation of 40h MM $Al_{64}Cu_{29}Fe_7Cr_8$ and $Al_{65}Cu_{20}Fe_7Mn_8$ alloys.

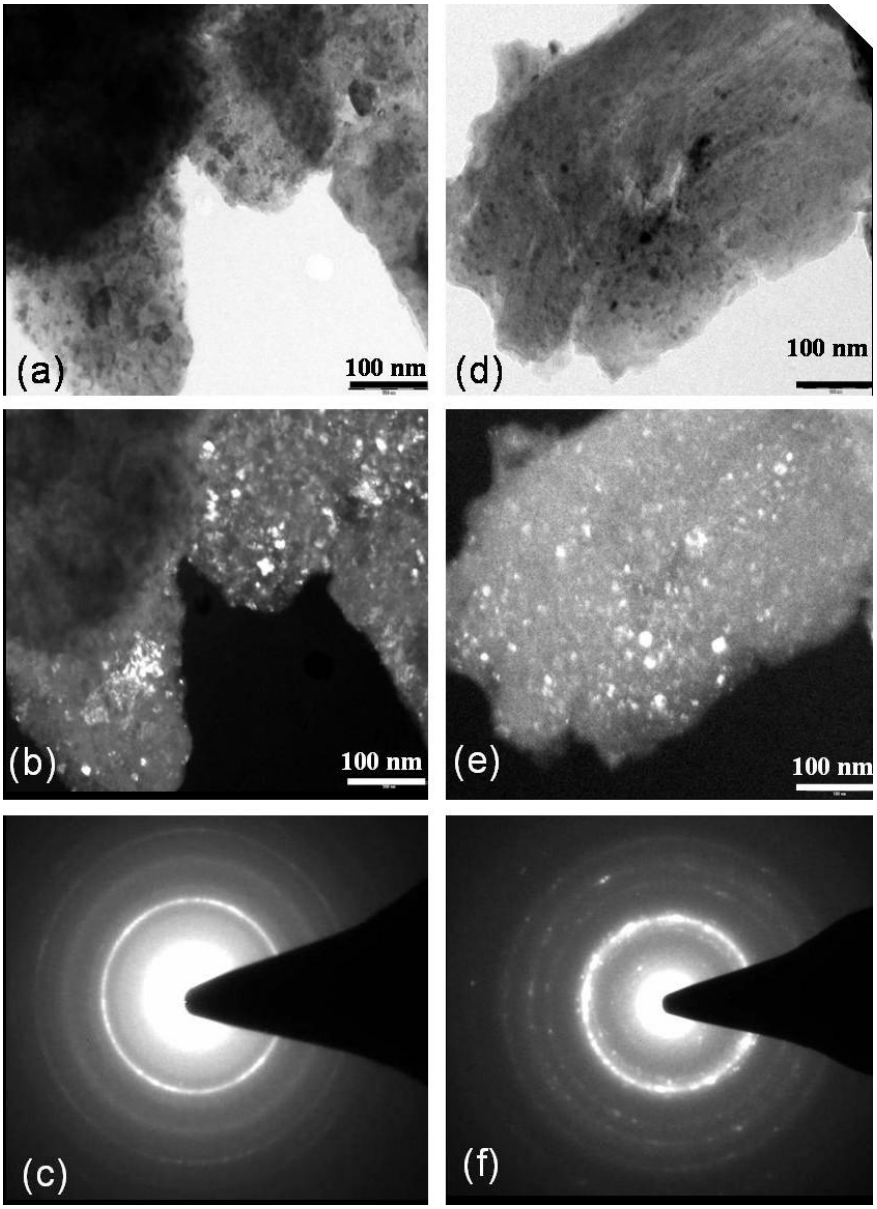

Figure 6. The bright field and dark field TEM microstructure of 40 h MM sample of $Al_{65}Cu_{20}Fe_7Cr_8$ (a-b) and the corresponding electron diffraction pattern in (c). The bright field and dark field TEM microstructure of 40 h MM $Al_{65}Cu_{20}Fe_7Mn_8$ alloy (d-e) and the corresponding electron diffraction patterns in (f).

The bright field and dark field microstructure of 40 h MM sample of $Al_{65}Cu_{20}Fe_7Cr_8$ can be seen in Fig. 6(a-b). Very fine equiaxed particles of the nanometer size (~20 nm) are visible. The corresponding electron diffraction pattern, shown in Fig. 6(c) was indexed due to B2 phase. Fig. 6 (d-e) shows a bright field and dark field TEM micrograph of 40 h MM $Al_{65}Cu_{20}Fe_7Mn_8$ alloy. The large number of small size particles embedded in the big grain in lamellar microstructure can easily be discerned in the Figure 6(d-e). The average particle size is of ~16-24 nm. The corresponding electron diffraction patterns are shown in Fig.6 (f). All the diffraction rings are indexed in the terms of B2 phase with lattice parameter of 2.92 Å. This lattice parameter agrees reasonably well with the XRD results.

HRTEM images of 40 h MM and 60 h annealed $Al_{65}Cu_{20}Fe_7Cr_8$ powder (Figures 7 (a)) clearly show the lattice resolution image of the nanocrystalline spinel phase along (111) plane. The appearance of amorphous like region is due to the presence of formvar used as mounting material in Cu grid. The

HRTEM image of $Al_{65}Cu_{20}Fe_7Mn8$ 40 h MM alloy followed by annealing at 900 ^oC for 60 h in air (Fig.7 (b)) clearly shows the same type lattice image of spinel phase as mentioned earlier. In this case very sharp fringes along (111) plane indicating the ordering has been observed.

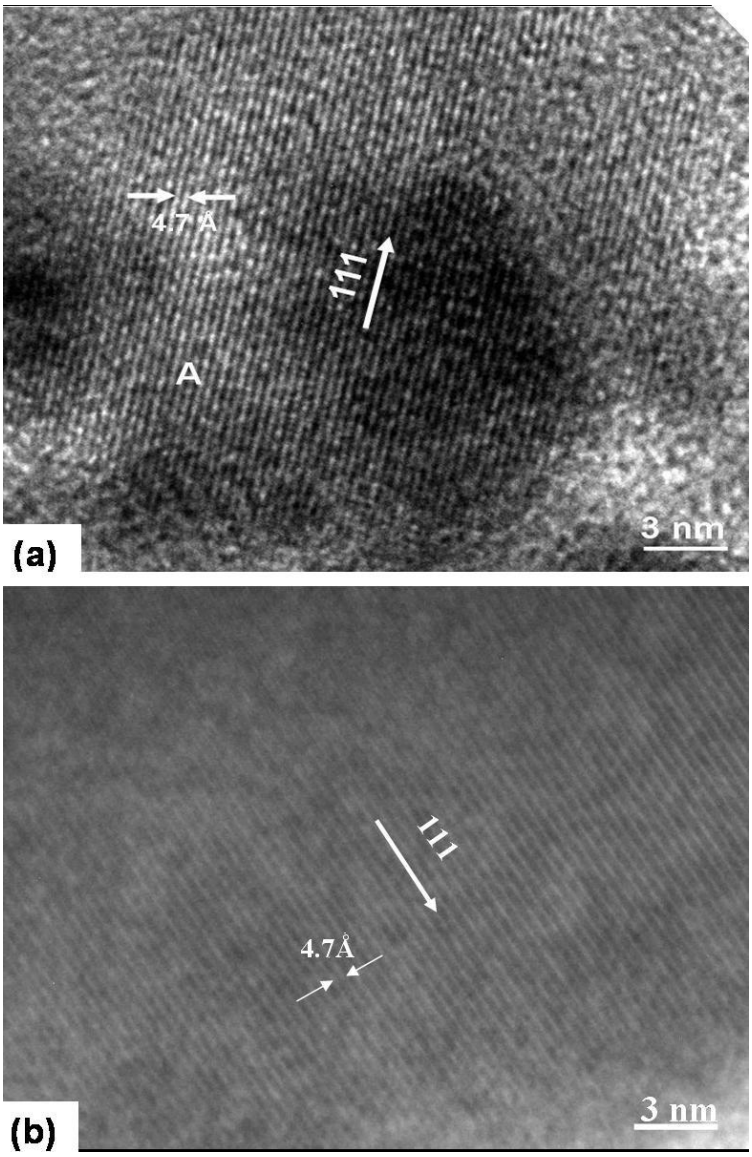

Figure 7. HRTEM images of 40 h MM and 60 h annealed $Al_{65}Cu_{20}Fe_7Cr_8$ powder (a) and $Al_{65}Cu_{20}Fe_7Mn_8$ 40 h MM alloy followed by annealing at 900 oC for 60 h in air (b).

4. Conclusions

It is clear from the present investigation that after milling the decagonal and 1DQC quasicrystal in $Al_{64}Cu_{29}Fe_7Cr_8$ and $Al_{65}Cu_{20}Fe_7Mn_8$ alloy have transformed to the crystalline phase (i.e., disordered B2 phase) with a nanoscale microstructure of 20 nm approximately. At the initial stage of milling (10h) of $Al_{64}Cu_{29}Fe_7Cr_8$ alloy, the decagonal phase transforms to an icosahedral phase which further transformed to B2 phase. In both the cases the evolution of the spinel structure started upon air annealing at 600 °C from the B2 phase formed due to milling of quasicrystalline phases for 40h but $Al_{65}Cu_{20}Fe_7Mn_8$ alloy is more stable compare to $Al_{64}Cu_{29}Fe_7Cr_8$ alloy. From the analysis it appeared that Al-Cu-Fe-Cr decagonal phase exhibits better spinel forming ability compared to that of Al-Cu-Fe-Mn 1DQC. This could be due to the initial structure as well as the higher affinity of Cr for oxygen compared to that of Mn.

Acknowledgement
The authors would like to thank Prof G.V.S. Sastry, Prof. R.K. Mandal, and Dr. M.A.Shaz, for discussions. The authors also gratefully acknowledge the Department of Science and Technology (DST), New Delhi and the Ministry of New-Renewable Energy, New Delhi, India for financial support.

References

[1] Shechtman D, Blench I, Gratias D and Cahn J W 1984 *Phys Rev. Lett***, 53** 1951
[2] Tsai A P, Inoue A, Masumoto T and Kataoka N 1988 *Jpn. J. Appl. Phys.* **27** L2252
[3] Poon S J, Drehman A J and Lawless K R 1985 *Phys. Rev. Lett.* **55** 2324
[4] Tsai A P, Inoue A and Masumoto T 1989 *Mater. Trans. Jpn. Inst. Met.* ***30*** 150
[5] Archambault P and Janot C 1997 *Mater. Res. Soc. Bulletin.****22*** 48
[6] Mancinelli Chris, Ko1 J S and Jenks C J 2001 *Mat. Res. Soc. Symp. Proc.* **643** K821
[7] McGrath R, Ledieu J, Erik Cox J and Renee Diehl D 2002 *J. Phys.: Condens. Matter.* ***14*** R119
[8] Besser MF and Eisenhammer T 1999 *Mater.Res. Soc. Bulletin, **722*** 59
[9] Urban K, Feuerbacher M and Wollgarten M 1997 *Mater.Res. Soc. Bulletin.* ***22*** 65
[10] Kelton K F and Gibbons P C 1997 *Mater.Res. Soc. Bulletin.* ***22*** 69
[11] Tiwari RS,Yadav TP, Mukhopadhyay NK and Srivastava O N 2009 *Z. Kristallogr.* ***224*** 26
[12] Elina Huttunen-Saarivirta 2004 *Journal of Alloys and Compounds* ***363*** 150
[13] Yadav T P, Mukhopadhyay N K, Tiwaria R S and Srivastava O N 2005 *Trans. IIM* ***58*** 1169
[14] Dong C and Dubois J M 1991 Journal of materials science **26** 1647
[15] Tsai A P, Sato A, Yamamoto A,Inoue A and Masumoto T 1992 *J. App Phys* ***31*** L970
[16] Mukhopadhyay N K,Yadav T P,Tiwari R S and Srivastava O N 2008 *Z. Kristallogr.* ***223*** 716
[17] Yadav TP, Mukhopadhyay N K, Tiwari RS and Srivastava O N. 2005 *Mater. Sc. Eng.A* ***393*** 366
[18] Mukhopadhyay NK and Loard E A 2002 *Acta. Cryst. A.* ***58*** 424